Mitigating Electrode Inactivation During CO_2 Electrocatalysis in Aprotic Solvents with Alkali Cations

Benjamin C. Kash,[†^] Reginaldo J. Gomes,[†^] and Chibueze V. Amanchukwu[†*]

[†]Pritzker School of Molecular Engineering, The University of Chicago, Chicago, IL, 60637

[^]B.K. and R.G. contributed equally to this work.

*Corresponding author

Email: chibueze@uchicago.edu

Abstract

CO_2 electrochemical reduction (CO_2R) in aprotic media is a promising alternative to aqueous electrocatalysis, as it minimizes the competing hydrogen evolution reaction while enhancing CO_2 solubility. To date, state-of-the-art alkali salts used as electrolytes for selective aqueous CO_2R are inaccessible in aprotic systems due to the inactivation of the electrode surface from carbonate deposition. In this work, we demonstrate that an acidic non-aqueous environment enables sustained CO_2 electrochemical reduction with common alkali salts in dimethyl sulfoxide. Electrochemical and spectroscopic techniques show that at low pH, carbonate build-up can be prevented, allowing CO_2R to proceed. Product distribution with a copper electrode revealed up to 80% faradaic efficiency for CO_2R products, including carbon monoxide, formic acid, and methane. By understanding the mechanism for electrode deactivation in an aprotic medium and addressing that challenge with dilute acid addition, we pave the way toward the development of more efficient and selective electrolytes for CO_2R.

Introduction

Rising carbon dioxide (CO_2) emissions has galvanized interest in the capture and utilization of CO_2 for desired carbon-containing products, such as fuels and basic chemicals. As renewable energy technologies such as solar and wind reach cost parity with fossil fuels, the electrochemical reduction of CO_2 (CO_2R) becomes an attractive option for obtaining value from CO_2[1–3]. Low-temperature CO_2 electrocatalysis is conventionally conducted in an aqueous environment with a heterogenous metal catalyst[4,5]. However, aqueous CO_2R is limited by the competitive hydrogen evolution reaction from water breakdown, which occurs at similar potentials to CO_2 reduction[6,7]. In many reported systems, HER dominates the CO_2R at a wide range of applied potentials[6,7]. Using an aprotic, non-aqueous solvent such as acetonitrile (ACN) or dimethylsulfoxide (DMSO) holds promise for suppressing HER since aprotic media do not contain easily reduced protons[8,9]. Aprotic solvents enable higher concentrations of dissolved CO_2 and enhanced CO_2 mass transport compared to aqueous media[10,11]. In addition, the tunability of the aprotic solvent allows for probing solvent effects and allows one to separate the proton source (e.g., water) from solvent effects, enabling a better mechanistic understanding of CO_2R.

For aqueous CO_2R, alkali cations such as K^+ and Cs^+ are the most commonly used supporting ions, as they enable high ionic conductivities and support the formation of valuable multi-hydrogenated C2+ products such as ethylene, ethanol, n-propanol etc[12–14]. However, when alkali salts are used for CO_2R in aprotic solvents, no products are observed. Instead, there is a complete suppression of the current densities. This phenomenon has been reported by different authors[15,16], with some attributing it to the formation of a 'hydrophilic layer'[17] and others a 'deactivation film'[18]. Recently, through experimental investigation of the electrode interface, we reported the formation of an insoluble alkali carbonate passivation layer at the electrode surface that suppresses further CO_2R[19]. Carbonate is an inherent side product of CO_2R in both aqueous and non-aqueous media[20,21]. In aqueous media, carbonates remain soluble, meaning electrolysis continues despite this side reaction. However, in an aprotic environment, carbonate precipitates in the presence of harder cations (such as alkalis), passivating the reactive electrode surface and leading to a cessation of CO_2R[19]. Therefore, all reported CO_2R in aprotic media use ammonium-based cations or ionic liquids that produce soluble carbonates. Since the formation of C2+ products in aqueous media have partly been attributed to the presence of alkali cations, it lends the question: is the lack of

C2+ products in aprotic media due to the lack of dissolved alkali cations? Unfortunately to date, there have been no reported strategies to avoid electrode inactivation and enable sustained CO_2R in an alkali-containing aprotic media.

In this work, we use a diluted acid mixture to prevent carbonate formation and enable CO_2R with alkali cations for the first time in an aprotic medium. To lower the electrolyte pH, methanesulfonic acid (MSAc) was chosen due to its dissolution and strength in an aprotic solvent such as dimethylsulfoxide (DMSO). We studied the CO_2 electrochemical reduction process and product distribution for a variety of alkali-containing perchlorate salts. In an acidic, non-aqueous environment, carbonate formation was successfully avoided, and product distribution experiments demonstrated access to CO_2R products with up to 80% total faradaic efficiencies with different alkali salts. X-ray photoelectron spectroscopy (XPS) and nuclear magnetic resonance spectroscopy (NMR) were leveraged to probe the CO_2 speciation on both electrode surfaces and bulk solution, respectively.[22] Results of this work greatly expand the available electrolyte design space for study within aprotic, non-aqueous media and provides a route to investigate state-of-the-art salts that have been used for aqueous CO_2R.

Results and Discussion

Probing electrode reactivation during CO_2R using an acidic medium

The effect of a Li^+-containing electrolyte on suppressing CO_2R in an aprotic medium is shown in the voltammograms in Figure 1a. In our prior work, we used 1,2-dimethoxyethane, a solvent with a low dielectric constant and significant ion pairing[19]. Here, we use dimethylsulfoxide (DMSO) to enable improved salt dissolution and higher ionic conductivities. In the absence of acid, no significant cathodic current is observed up to -2.5V vs decamethylferrocene (Fc*), where Li^+ reduction begins. However, the addition of 50mM MSAc resulted in the appearance of two new reductive features at -0.8V and -1.6V that we attribute to proton and CO_2 reduction, respectively. All potentials are referenced to decamethylferrocene (Fc*) unless otherwise stated. Phosphoric acid (H_3PO_4) was also investigated but was unable to maintain CO_2R up to concentrations of 250mM; an observation we attribute to its weaker acidity (Figure S1). To ensure that the changes

are not due to water effects, $CsClO_4$ electrolyte concentrated with 500 mM H_2O was also tested (Figure S2) and it was unable to sustain CO_2R. The absence of CO_2R indicates that the presence of H_2O alone is also insufficient to maintain CO_2R within a bulk non-aqueous electrolyte containing alkali cations.

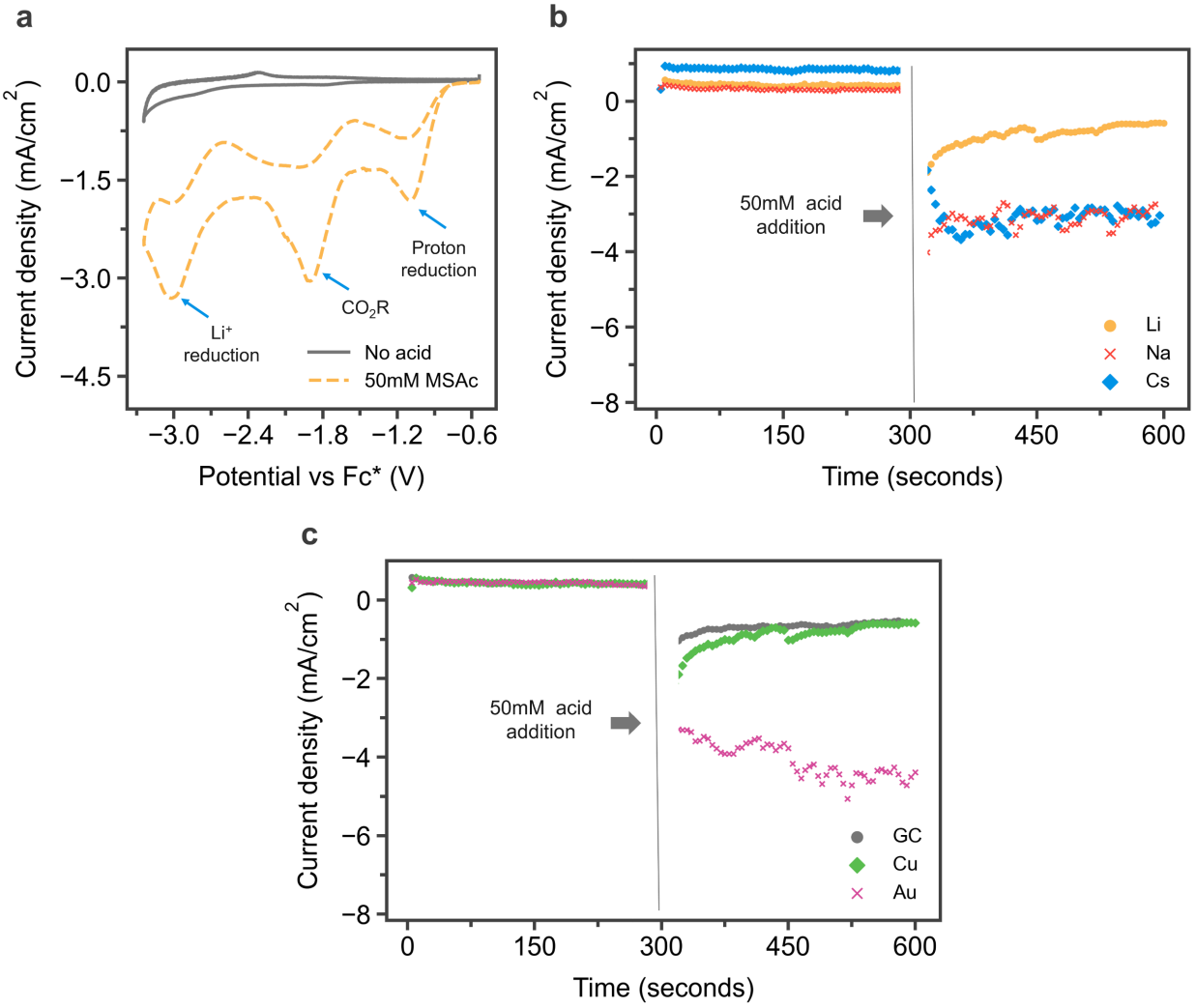

Figure 1. (**a**) Cyclic voltammetry for a 0.1M $LiClO_4$, CO_2 saturated solution in DMSO with Au electrode at 50 mV/s without acid (solid line) and with 50mM MSAc (dashed); (**b**) Chronoamperometry data for 0.1M $LiClO_4$, $NaClO_4$, and $CsClO_4$ electrolytes for a Cu electrode at a potential of -2.4 V vs Fc* before and after the addition of 50 mM MSAc; and (**c**) Chronoamperometry data for 0.1M $LiClO_4$ electrolyte over Au, GC (glassy carbon), and Cu electrodes. MSAc = methanesulfonic acid. Fc* = decamethylferrocene.

To further investigate the electrode deactivation process, we performed CO_2R under acidic conditions across different electrodes and electrolyte salts. As shown in Figure 1b, no cathodic current is observed at -2.4V vs Fc* across different alkali perchlorate salts ($LiClO_4$, $NaClO_4$, and $CsClO_4$) in the absence of acid. After the addition of 50mM MSAc, all systems could sustain current densities around 1mA/cm^2 and greater. Similar behavior was also observed during CO_2R over gold and glassy carbon electrodes (Figure 2c), indicating that the electrode deactivation process is independent of the heterogeneous catalyst.

The effect of the electrolyte on the electrode surface chemistry was further investigated through XPS analysis of the Cu electrodes after CO_2R. For all electrolytes (Figure 2), we can observe peaks at 284.4, 285.2, and 288.5 eV corresponding to C-C, C-O, and C=O, respectively[23]. These peaks were also observed in the C1s spectrum taken as a control on pristine Cu foil (Figure S3). Under neutral conditions (Figure 2a-c), all alkali electrolytes presented an additional peak centered around 289.6 eV, indicating the presence of inorganic carbonates deposit (CO_3^{2-}) over the electrode surface[24]. However, these new peaks completely disappear when acid is added during the electrochemistry (Figure 2d-e). These results indicate that the precipitation of carbonate species in the presence of alkali cations may be the main cause of the immediate drop in current and eventually cessation of CO_2R in a non-aqueous medium. This decay in electrochemical

performance has also been observed in different electrochemical systems, where carbonate precipitation results in poor rechargeability of metal-CO_2 and metal-O_2 batteries.[25,26]

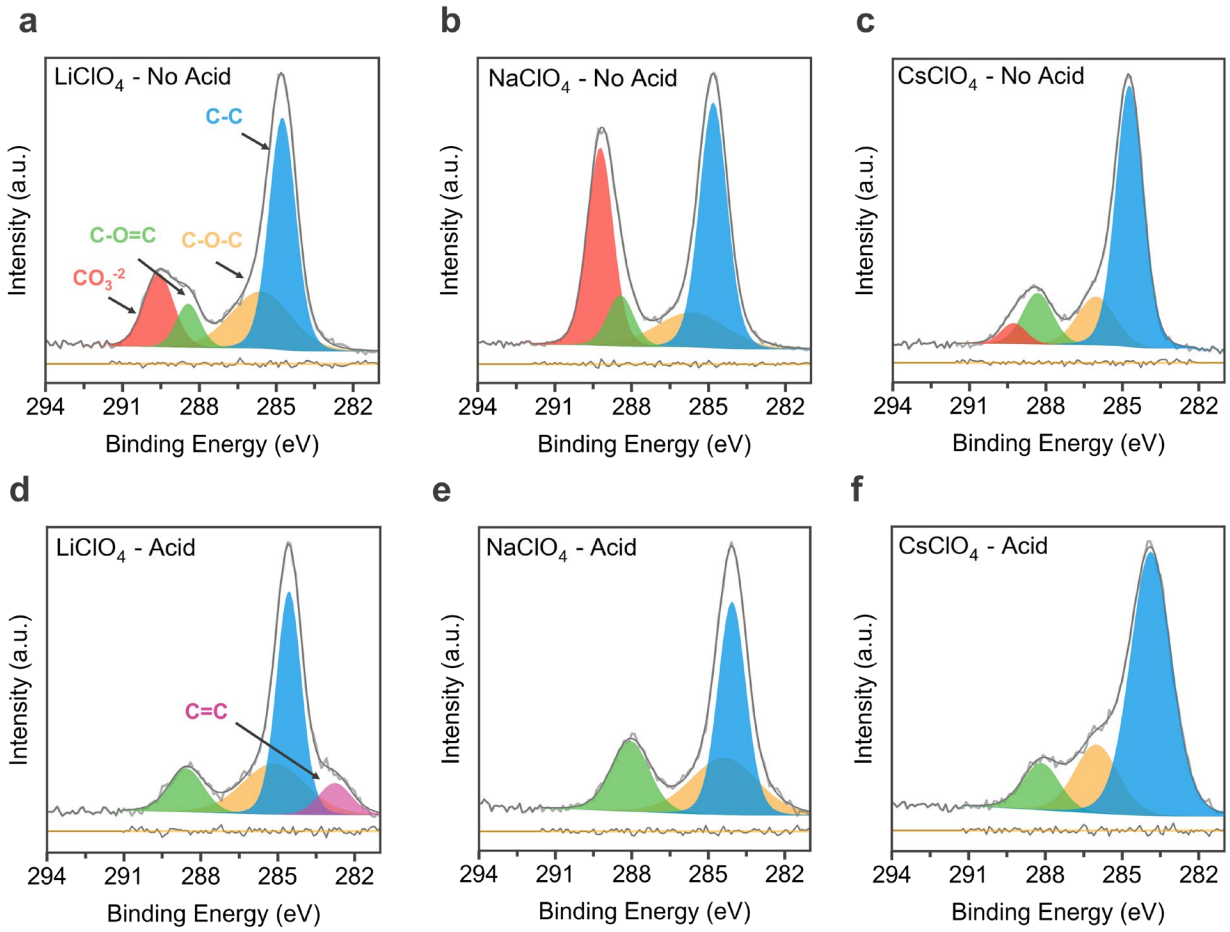

Figure 2. C1s spectra from XPS analysis of a Cu foil after 10min electrolysis at -2.4V vs Fc* in a CO_2 saturated solution containing (**a**) 0.1 M $LiClO_4$, (**b**) 0.1M $NaClO_4$, (**c**) 0.1M $CsClO_4$, (**d**) 0.1 M $LiClO_4$ and 50mM MSAc, (**e**) 0.1M $NaClO_4$ and 50mM MSAc, and (**f**) 0.1M $CsClO_4$ and 50mM MSAc.

Investigating the CO_2 speciation in a non-aqueous medium

Carbonate formation is an inherent side reaction of CO_2R which continues to be a major obstacle to improving the carbon and energy efficiencies of this technology[20]. In an aqueous medium, it is formed by the equilibrium between the dissolved CO_2 and the *in situ* generated OH^- (Equation 1).

In an aprotic medium, carbonate is formed by the disproportionation of CO_2 molecules undergoing electrochemical reduction (Equation 3)[27]. Nevertheless, as seen in Equation 2, carbonate may also remain in equilibrium with HCO_3^- when small amounts of water are present in the electrolyte as demonstrated elsewhere[15,28].

Carbonate Formation in Aqueous Medium[29]

$$CO_2 + H_2O + 2e^- \rightarrow COOH_{ad} + OH^- + e^- \rightarrow CO + 2OH^- \quad (1)$$

$$CO_2 + H_2O \leftrightharpoons HCO_3^- + OH^- \leftrightharpoons CO_3^{2-} + H_2O \quad (2)$$

Carbonate Formation in an Aprotic Medium[21]

$$CO_2 + CO_2 + 2e^- \rightarrow {C_2O_4}^{2-} \rightarrow CO + CO_3^{2-} \quad (3)$$

Here, we used ^{13}C-NMR to probe the $^{13}CO_2$ speciation in a non-aqueous environment in the presence of alkali cations. Figure 3 shows the ^{13}C NMR spectra of pristine DMSO saturated with isotopically enriched $^{13}CO_2$ where we observe a peak at 125 ppm assigned to CO_2[30,31]. The presence of 0.1M $LiClO_4$ in the saturated solution does not promote any change in CO_2 speciation. However, the addition of 5mM TBAOH•30H_2O results in the appearance of a new peak at 158 ppm, which is assigned to the formation of HCO_3^-.[31,32] TBAOH was used to mimic the increase in solution pH during CO_2R[33]. The bicarbonate then arises from the increase in apparent pH from around 9.5 to 13.5, which shifts the CO_2 equilibrium. These species remains soluble in an aprotic medium in the presence of the quaternary ammonium cation[19,28]. However, the addition of 50mM MSAc to the HCO_3^--containing solution brings the apparent pH down to values around 3-4. Under acidic conditions, the HCO_3^- equilibrium shifts to the formation of CO_2, and the peak at 158 ppm is no longer observed. The addition of 0.1M $LiClO_4$ also promotes the HCO_3^- peak disappearance, but it cannot be explained by a change in the solution pH, since it still remains basic (around 13-14). Instead, Li^+ promotes the precipitation of the (bi)carbonates, as previously indicated by the XPS results in Figure 2.

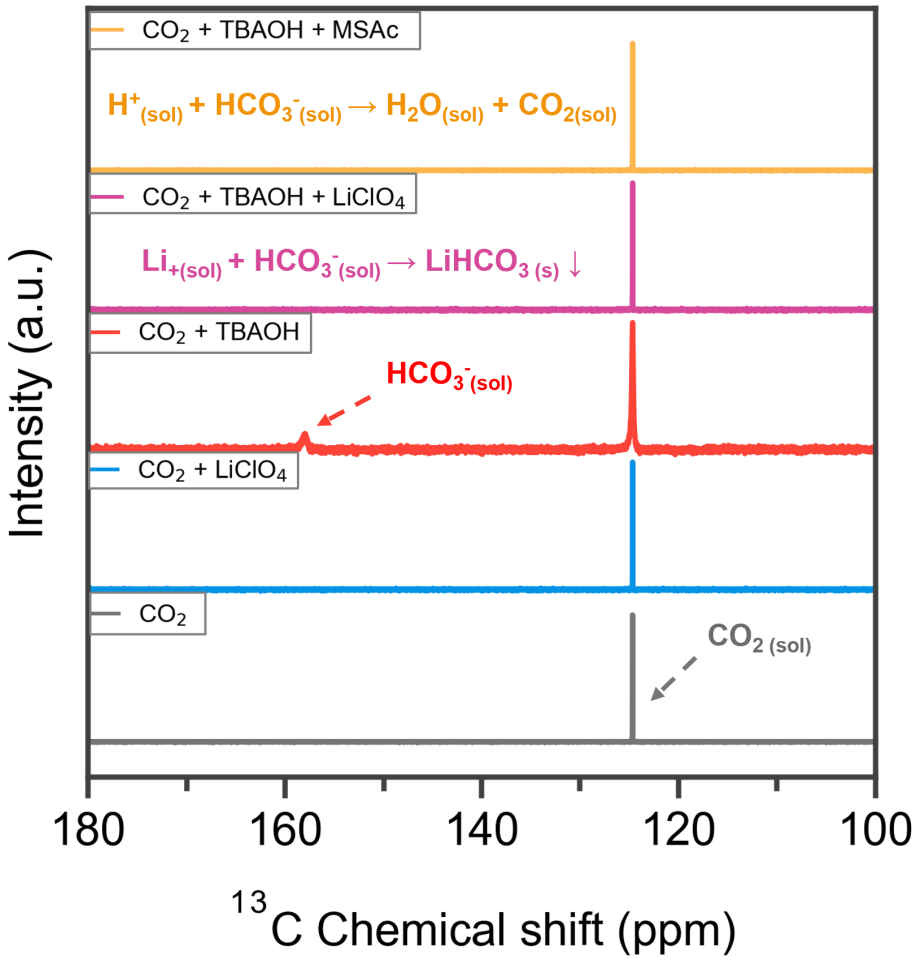

Figure 3. (a) ^{13}C NMR spectra of $^{13}CO_2$ saturated solutions in pristine DMSO (gray), and DMSO containing 0.1M $LiClO_4$ (red), 5mM $TBAOH^{\bullet}30H_2O$ (blue); 5mM $TBAOH^{\bullet}30H_2O$ after the addition of 50mM MSAc (yellow), and 0.1M $LiClO_4$ (purple).

Based on our studies on CO_2 speciation in the bulk solution and at the electrode surface, we can now propose a mechanism to explain the effect of carbonate on CO_2R performance in an aprotic medium. As depicted in Figure 4**,** in neutral to alkaline electrolytic media (apparent pH > 7), carbonate species will immediately precipitate after reacting with any available alkali cation in a nonaqueous environment. Since carbonate species are generated *in situ* during CO_2R, this process occurs near the electrode surface leading to the formation of an insulation layer that prevents additional electron transfer to the CO_2 molecules. As a result, the electrode is quickly deactivated. This deactivation process can be circumvented by shifting the electrolyte pH to an acidic

environment, where the presence of protons in the bulk will convert the (bi)carbonate back into its CO_2 form[25]. A lack of carbonate species means no passivation will occur at the electrode surface and CO_2R can be sustained even in the presence of alkali-containing electrolytes. Given that protons are stochimetrically generated by the oxygen evolution reaction (OER) on the anolyte side and can be delivered through a proton exchange membrane (PEM), there will be continual supply of protons delivered to the electrode to eliminate carbonate species. Therefore, this setup provides a realistic method for performing low pH, non-aqueous CO_2R at scale.

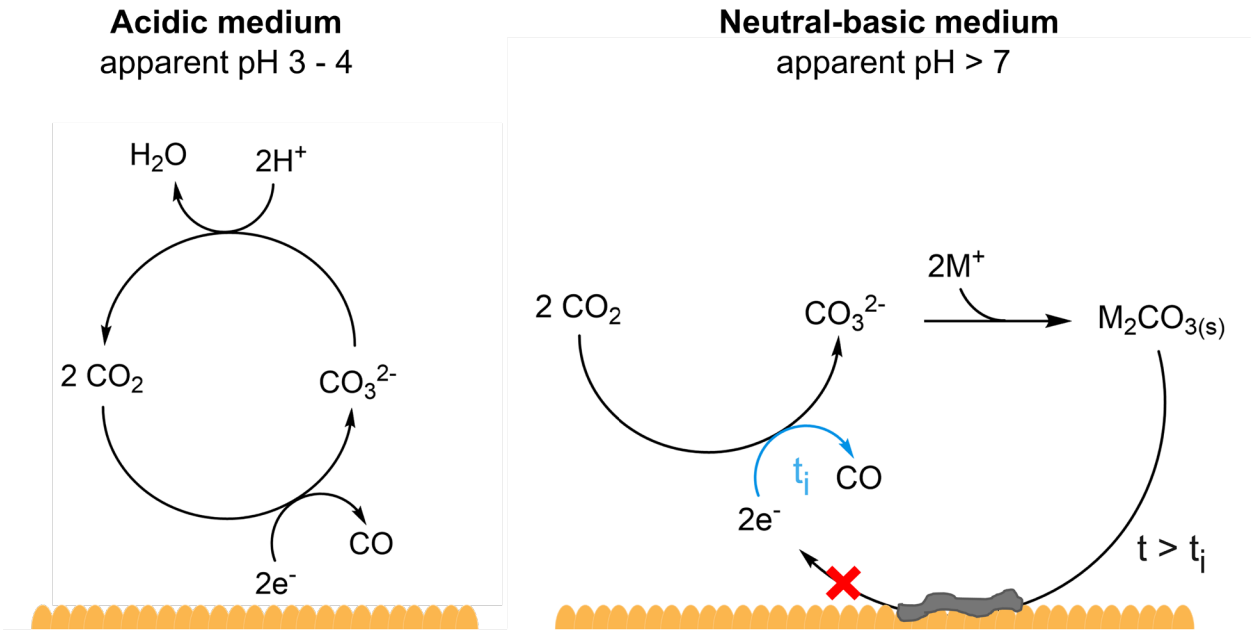

Figure 4. Summary of CO_2 speciation during CO_2R in the presence of an alkali cation (M^+) in a non-aqueous medium in both acidic and neutral-basic conditions. t_i = initial time

CO_2R product distribution experiments

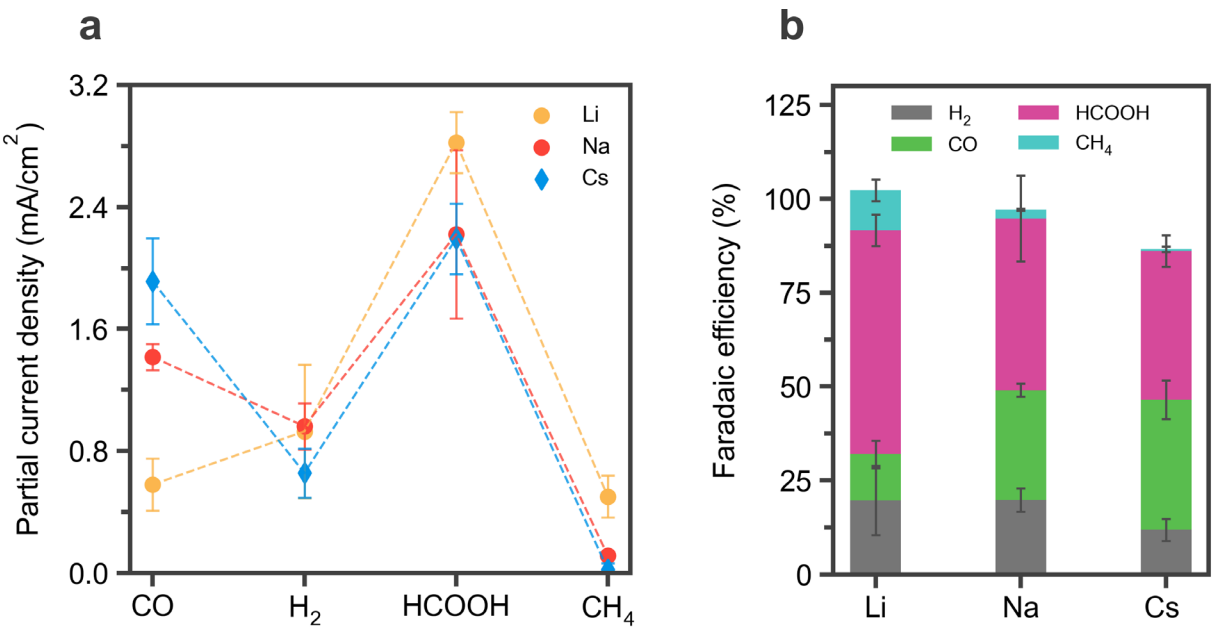

Figure 5. (a) Partial current densities for the different products and (**b**) product distributions Faradaic efficiencies for CO_2R as a function of alkali cations with 50mM MSAc in DMSO. Experiments were conducted over a Cu working electrode at -2.1V vs Fc*. The dashed lines in (a) are to guide the eyes. Salt concentration (0.1M perchlorate salts).

The product distribution of CO_2R using alkali salts in DMSO was investigated using an H-Cell setup. The gaseous products were quantified with gas chromatography, while the liquid phase products were quantified using ^{1}H NMR. A copper electrode was used since it can provide a wide range of CO_2R products in an aprotic nonaqueous medium, such as formic acid, carbon monoxide, and methane[9, 15,19]. As shown in Figure 5**,** different CO_2R products were observed when in the presence of Li, Na and Cs containing electrolytes. To the author's knowledge, this shows the first time in which alkali cations have successfully been used for CO_2R within an aprotic solvent.

The CO_2R product distribution was significantly affected by the nature of the electrolyte. As shown in Figure 5a, carbon monoxide partial current density increases with the size of the alkali cation, reaching FE values up to 40% for Cs containing electrolytes (Figure 5b). On the other hand, formic acid accounted for almost 60% of the product distribution when lithium is present. Methane can also be observed with faradaic efficiency (FE) values of around 10% only for the lithium-

containing electrolyte. Nevertheless, hydrogen FE seems to be electrolyte independent, accounting for between 15-20% of the FE for all electrolytes. Tests conducted under Argon atmosphere show hydrogen as the main product (Figure S4), thus indicating that the carbon containing products observed here are exclusively from CO_2R and not electrolyte decomposition. Our results demonstrate successfully sustained electrocatalysis of CO_2R within a non-aqueous media using alkali-containing electrolytes. This shows that aprotic solvents offer high faradaic yields toward valuable CO_2R products in low pH conditions without requiring high operating current densities[33,34] or complex electrode materials[35] which are required to access similar yields in aqueous media.

By varying the cation present we may tune the CO_2R products such as CO and HCOOH, as well as enable access to multi-hydrogenated products such as methane. Although we observe a variety of products, no C2+ species are present. This indicates that alkali cations alone are not responsible for C2+ product formation, but rather, a confluence of cation, solvent, proton effects, along with catalyst design contribute to CO_2R product distributions. Further investigation of these factors will be needed to understand the effects on catalyst surface and the reasons why.

Conclusions

In this work, we investigated and addressed electrode deactivation that occurs when performing CO_2 electrocatalysis with alkali-containing electrolytes in aprotic media. Our XPS and ^{13}C-NMR experiments revealed that the *in situ* generated carbonate is responsible for the formation of an insulating layer on the electrode surface when in the presence of any alkali cation. This process results in an immediate drop in current density and electrode deactivation. To circumvent this issue, the addition of a dilute methanesulfonic acid was used to shift the CO_3^{2-} equilibrium back into CO_2, preventing carbonate deposition. Product distribution analysis under these acidic conditions showed the formation of carbon monoxide, formic acid, and methane and their dependence on the electrolyte composition. CO production increases with the size of the cation present in the electrolyte, while Li favors the production of formic acid and methane. Results from work will help in the design of novel alkali-based electrolytes for CO_2R in a nonaqueous environment.

Experimental Section

Materials

Lithium perchlorate (>95%) was purchased from Oakwood Chemicals. Cesium perchlorate (99%) was purchased from Thermo Fischer. Sodium perchlorate (98%) and Methanesulfonic acid (> 99.0%) were purchased from Millipore Sigma. Nafion N-117 proton exchange membrane (0.18mm thick, 0.9 meq/g exchange capacity) and tetra-n-butylammonium perchlorate (99%) were purchased from Alfa-Aesar. Dimethyl sulfoxide (anhydrous, 99.9%) and formic acid (98-100%) were purchased from Sigma Aldrich. Solvents were stored in argon filled VigorTech glove box (H_2O and O_2 < 1 ppm). NMR experiments were performed with deuterated dimethyl sulfoxide (>99.8% atom %D) purchased from Cambridge Isotope Laboratories. Phenol was purchased from Acros Organics. All chemicals used as received. Both carbon dioxide (99.9995%) and argon (99.999%) gases were purchased from Airgas. Copper disk electrode (7.07 mm^2) created by fitting super-conductive copper rods (99.999% metal basis, Puratronic™) into a PEEK tubing. Platinum foil 99.99% (Beantown chemical) was used as a counter electrode. Gold disk electrode (7.07 mm^2), glassy carbon electrode (7.07 mm^2), and Ag/AgCl reference electrode were purchased from eDAQ.

Electrochemical characterization

Studies were performed using a three-electrode configuration beaker electrochemical cell (Figure S5) with a miniature, leakless Ag/AgCl as the reference electrode, a platinum (Pt) foil as the counter electrode, and copper (Cu), gold (Au), or glassy carbon (GC) (7.07 mm^2) disk electrodes used as the working electrode. Working electrodes were prepared by soaking in 0.5 M sulfuric acid solution then polishing with an alumina suspension and rinsing with Milli-Q water (18.4 MΩ/cm). Electrolyte solution contained 50mM of perchlorate salt in DMSO, with the addition of 50mM methanesulfonic acid (MSAc) for acidic pH trials. CO_2 or Argon was bubbled into the electrolyte solution for 5 min before electrochemical experiments began. A Biologic VSP Potentiostat was used for all electrochemical experiments.

pH measurements

pH measurements were taken with a Mettler-Toledo SevenCompact pH Meter. Measurements were taken in a non-aqueous media; therefore, the results are reported as "apparent pH" since they are not calibrated to the aqueous scale.

Product analysis using gas chromatography and ^{1}H NMR spectroscopy

CO_2R reactions performed in a symmetric H-cell setup (Figure S6) with an Ag/AgCl as the reference electrode, a platinum (Pt) foil as the counter electrode, and copper (Cu) or gold (Au) disk electrodes used as the working electrode. Electrolyte for both catholyte and anolyte compartments contained 50mM $CsClO_4$ in DMSO, with the addition of 50mM methanesulfonic acid (MSAc) for acidic trials. Compartments separated by Nafion N-117 proton exchange membrane. Inlet tubing is used to bubble either CO_2 or Ar into the catholyte solution at a constant flow rate of 20 sccm. Bubble formation on the electrode surface was minimized through tubing placement. The solution was bubbled for 5 minutes with either gas before a potential was applied. The catholyte solution was stirred at 500 rpm. Gaseous products were identified and quantified with a Shimadzu GC-2014 gas chromatograph using both a flame ionization detector (FID) and a thermal conductive detector (TCD). Liquid phase products were analyzed using a Bruker Ascend 9.4 T/400 MHz instrument for ^{1}H NMR spectroscopy. Formic acid identification through ^{1}H NMR and calibration curve implemented for formic acid quantification are shown in Figures S6 and S7.

XPS characterization

X-ray photoelectron spectroscopy was performed on copper foil strips (1 x 1cm) which were used as working electrodes within beaker cell electrochemical experiments. The platinum foil was used as a counter electrode, and Ag/AgCl was used as a reference electrode. Following electrolysis, foils were carefully removed and rinsed three times with DMSO and then allowed to dry under ambient conditions. XPS experimentation was conducted on a Kratos Axis Nova spectrometer based on an Al Ka radiation source (hv = 1486.6 eV, 100 µm, 25 W) with a delay line detector (DLD). XPS samples were referenced to 284.8 eV, corresponding to the C-C component of the C1s spectrum. Peak deconvolution and fitting were performed with the CasaXPS software [36]. Shirley's background correction was used.

CO_2-speciation studies

^{13}C labeled carbon dioxide (99 atom % ^{13}C, 99.93 atom % ^{16}O, Millipore Sigma) was purged for 5min at 5sccm into 2ml of sample. Carbonate was identified using ^{13}C NMR in a Bruker Ascend 9.4 T/400 MHz instrument.

Acknowledgments

This work was supported by generous start-up funds from the University of Chicago, the Neubauer Family Assistant Professors program, and the CIFAR-Azrieli Global Scholars Program. Additionally, B.K. was supported by the Astronaut Scholarship Foundation and the Jeff Metcalf Internship Program. We thank Alexander Filatov for performing the XPS measurements.

Supporting Information

XPS results, material and methods for electrochemical characterization and product distribution analysis, and additional figures.

References

(1) Shin, H.; Hansen, K. U.; Jiao, F. Techno-Economic Assessment of Low-Temperature Carbon Dioxide Electrolysis. *Nat Sustain* **2021**, *4* (10), 911–919. https://doi.org/10.1038/s41893-021-00739-x.

(2) Phil, D. L.; Christopher, H.; Drew, H.; A, J. S.; F, J. T.; H, S. E. What Would It Take for Renewably Powered Electrosynthesis to Displace Petrochemical Processes? *Science (1979)* **2019**, *364* (6438), eaav3506. https://doi.org/10.1126/science.aav3506.

(3) Jordaan, S. M.; Wang, C. Electrocatalytic Conversion of Carbon Dioxide for the Paris Goals. **1929**. https://doi.org/10.1038/s41929-021-00704-z.

(4) Noda, H.; Ikeda, S.; Oda, Y.; Imai, K.; Maeda, M.; Ito, K. Electrochemical Reduction of Carbon Dioxide at Various Metal Electrodes in Aqueous Potassium Hydrogen Carbonate Solution. *Bull Chem Soc Jpn* **1990**, *63* (9), 2459–2462.

(5) Birdja, Y. Y.; Pérez-Gallent, E.; Figueiredo, M. C.; Göttle, A. J.; Calle-Vallejo, F.; Koper, M. T. M. Advances and Challenges in Understanding the Electrocatalytic Conversion of Carbon Dioxide to Fuels. *Nat Energy* **2019**, *4* (9), 732–745. https://doi.org/10.1038/s41560-019-0450-y.

(6) Ooka, H.; Figueiredo, M. C.; Koper, M. T. M. Competition between Hydrogen Evolution and Carbon Dioxide Reduction on Copper Electrodes in Mildly Acidic Media. *Langmuir* **2017**, *33* (37), 9307–9313. https://doi.org/10.1021/acs.langmuir.7b00696.

(7) Goyal, A.; Marcandalli, G.; Mints, V. A.; Koper, M. T. M. Competition between CO2 Reduction and Hydrogen Evolution on a Gold Electrode under Well-Defined Mass Transport Conditions. *J Am Chem Soc* **2020**, *142* (9), 4154–4161. https://doi.org/10.1021/jacs.9b10061.

(8) Amanchukwu, C. v. The Electrolyte Frontier: A Manifesto. *Joule* **2020**, *4* (2), 281–285. https://doi.org/https://doi.org/10.1016/j.joule.2019.12.009.

(9) Ikeda, S.; Takagi, T.; Ito, K. Selective Formation of Formic Acid, Oxalic Acid, and Carbon Monoxide by Electrochemical Reduction of Carbon Dioxide. *Bull Chem Soc Jpn* **1987**, *60* (7), 2517–2522. https://doi.org/10.1246/bcsj.60.2517.

(10) Gennaro, A.; Isse, A. A.; Vianello, E. Solubility and Electrochemical Determination of CO2 in Some Dipolar Aprotic Solvents. *J Electroanal Chem Interfacial Electrochem* **1990**, *289* (1), 203–215. https://doi.org/https://doi.org/10.1016/0022-0728(90)87217-8.

(11) König, M.; Vaes, J.; Klemm, E.; Pant, D. Solvents and Supporting Electrolytes in the Electrocatalytic Reduction of CO2. *iScience* **2019**, *19*, 135–160. https://doi.org/https://doi.org/10.1016/j.isci.2019.07.014.

(12) Monteiro, M. C. O.; Dattila, F.; Hagedoorn, B.; García-Muelas, R.; López, N.; Koper, M. T. M. Absence of CO2 Electroreduction on Copper, Gold and Silver Electrodes without Metal Cations in Solution. *Nat Catal* **2021**. https://doi.org/10.1038/s41929-021-00655-5.

(13) Ringe, S.; Clark, E. L.; Resasco, J.; Walton, A.; Seger, B.; Bell, A. T.; Chan, K. Understanding Cation Effects in Electrochemical CO2 Reduction. *Energy Environ Sci* **2019**, *12* (10), 3001–3014. https://doi.org/10.1039/C9EE01341E.

(14) Murata, A.; Hori, Y. Product Selectivity Affected by Cationic Species in Electrochemical Reduction of CO2 and CO at a Cu Electrode. *http://dx.doi.org/10.1246/bcsj.64.123* **2006**, *64* (1), 123–127. https://doi.org/10.1246/BCSJ.64.123.

(15) Figueiredo, M. C.; Ledezma-Yanez, I.; Koper, M. T. M. In Situ Spectroscopic Study of CO2 Electroreduction at Copper Electrodes in Acetonitrile. *ACS Catal* **2016**, *6* (4), 2382–2392. https://doi.org/10.1021/acscatal.5b02543.

(16) Neyrizi, S.; Kiewiet, J.; Hempenius, M. A.; Mul, G. What It Takes for Imidazolium Cations to Promote Electrochemical Reduction of CO 2. *ACS Energy Lett* **2022**, *14*, 3439–3446. https://doi.org/https://doi.org/10.1021/acsenergylett.2c01372.

(17) Berto, T. C.; Zhang, L.; Hamers, R. J.; Berry, J. F. Electrolyte Dependence of CO2 Electroreduction: Tetraalkylammonium Ions Are Not Electrocatalysts. *ACS Catal* **2015**, *5* (2), 703–707. https://doi.org/10.1021/cs501641z.

(18) Setterfield-Price, B. M.; Dryfe, R. A. W. The Influence of Electrolyte Identity upon the Electro-Reduction of CO2. *Journal of Electroanalytical Chemistry* **2014**, *730*, 48–58. https://doi.org/10.1016/J.JELECHEM.2014.07.009.

(19) Gomes, R. J.; Birch, C.; Cencer, M. M.; Li, C.; Son, S.-B.; Bloom, I. D.; Assary, R. S.; Amanchukwu, C. v. Probing Electrolyte Influence on CO2 Reduction in Aprotic Solvents. *The Journal of Physical Chemistry C* **2022**, *126* (32), 13595–13606. https://doi.org/10.1021/ACS.JPCC.2C03321.

(20) Rabinowitz, J. A.; Kanan, M. W. The Future of Low-Temperature Carbon Dioxide Electrolysis Depends on Solving One Basic Problem. *Nat Commun* **2020**, *11* (1), 5231. https://doi.org/10.1038/s41467-020-19135-8.

(21) Amatore, C.; Saveant, J. M. Mechanism and Kinetic Characteristics of the Electrochemical Reduction of Carbon Dioxide in Media of Low Proton Availability. *J Am Chem Soc* **1981**, *103* (17), 5021–5023. https://doi.org/10.1021/ja00407a008.

(22) Xu, K. Nonaqueous Liquid Electrolytes for Lithium-Based Rechargeable Batteries. *Chem Rev* **2004**, *104* (10), 4303–4417. https://doi.org/10.1021/CR030203G/.

(23) Morgan, D. J. Comments on the XPS Analysis of Carbon Materials. *C 2021, Vol. 7, Page 51* **2021**, *7* (3), 51. https://doi.org/10.3390/C7030051.

(24) Ni, M.; Ratner, B. D. Differentiating Calcium Carbonate Polymorphs by Surface Analysis Techniques—an XPS and TOF-SIMS Study. *Surface and Interface Analysis* **2008**, *40* (10), 1356–1361. https://doi.org/10.1002/SIA.2904.

(25) Xie, Z.; Zhang, X.; Zhang, Z.; Zhou, Z. Metal–CO2 Batteries on the Road: CO2 from Contamination Gas to Energy Source. *Advanced Materials* **2017**, *29* (15), 1605891. https://doi.org/https://doi.org/10.1002/adma.201605891.

(26) Xu, S.; Lau, S.; Archer, L. A. CO2 and Ambient Air in Metal–Oxygen Batteries: Steps towards Reality. *Inorg Chem Front* **2015**, *2* (12), 1070–1079. https://doi.org/10.1039/C5QI00169B.

(27) Gennaro, A.; Isse, A. A.; Severin, M.-G.; Vianello, E.; Bhugun, I.; Savéant, J.-M. Mechanism of the Electrochemical Reduction of Carbon Dioxide at Inert Electrodes in Media of Low Proton Availability. *Journal of the Chemical Society, Faraday Transactions* **1996**, *92* (20), 3963–3968. https://doi.org/10.1039/FT9969203963.

(28) Mendieta-Reyes, N. E.; Cheuquepán, W.; Rodes, A.; Gómez, R. Spectroelectrochemical Study of CO2 Reduction on TiO2 Electrodes in Acetonitrile. *ACS Catal* **2020**, *10* (1), 103–113. https://doi.org/https://doi.org/10.1021/acscatal.9b02932.

(29) Dunwell, M.; Yan, Y.; Xu, B. Understanding the Influence of the Electrochemical Double-Layer on Heterogeneous Electrochemical Reactions. *Curr Opin Chem Eng* **2018**, *20*, 151–158. https://doi.org/10.1016/j.coche.2018.05.003.

(30) Liger-Belair, G.; Prost, E.; Parmentier, M.; Jeandet, P.; Nuzillard, J. M. Diffusion Coefficient of CO2 Molecules as Determined by 13C NMR in Various Carbonated Beverages. *J Agric Food Chem* **2003**, *51* (26), 7560–7563. https://doi.org/10.1021/JF034693P/.

(31) Seravalli, J.; Ragsdale, S. W. 13C NMR Characterization of an Exchange Reaction between CO and CO2 Catalyzed by Carbon Monoxide Dehydrogenase. *Biochemistry* **2008**, *47* (26), 6770–6781. https://doi.org/10.1021/BI8004522/.

(32) Eftaiha, A. F.; Mustafa, F. M.; Alsoubani, F.; Assaf, K. I.; Qaroush, A. K. A Catecholamine Neurotransmitter: Epinephrine as a CO2 Wet Scrubbing Agent. *Chemical Communications* **2019**, *55* (24), 3449–3452. https://doi.org/10.1039/C8CC09572H.

(33) Huang, J. E.; Li, F.; Ozden, A.; Rasouli, A. S.; de Arquer, F. P. G.; Liu, S.; Zhang, S.; Luo, M.; Wang, X.; Lum, Y.; et al. CO2 Electrolysis to Multicarbon Products in Strong Acid. *Science (1979)* **2021**, *372* (6546), 1074–1078. https://doi.org/10.1126/science.abg6582.

(34) Bondue, C. J.; Graf, M.; Goyal, A.; Koper, M. T. M. Suppression of Hydrogen Evolution in Acidic Electrolytes by Electrochemical CO2Reduction. *J Am Chem Soc* **2021**, *143* (1), 279–285. https://doi.org//10.1021/jacs.0c10397.

(35) Wang, Z.; Hou, P.; Wang, Y.; Xiang, X.; Kang, P. Acidic Electrochemical Reduction of CO2 Using Nickel Nitride on Multiwalled Carbon Nanotube as Selective Catalyst. *ACS Sustain Chem Eng* **2019**, *7* (6), 6106–6112. https://doi.org//10.1021/acssuschemeng.8b06278.

(36) Fairley, N.; Fernandez, V.; Richard-Plouet, M.; Guillot-Deudon, C.; Walton, J.; Smith, E.; Flahaut, D.; Greiner, M.; Biesinger, M.; Tougaard, S.; et al. Systematic and Collaborative Approach to Problem Solving Using X-Ray Photoelectron Spectroscopy. *Applied Surface Science Advances* **2021**, *5*, 100112. https://doi.org/https://doi.org/10.1016/j.apsadv.2021.100112.